Carbon Trends 22 (2026) 100602

Contents lists available at ScienceDirect

Carbon Trends

journal homepage: www.elsevier.com/locate/cartre

Effects of tensile strain on the electronic structure of graphene nanomesh

Prosun Santra [a], Michael Schlegel [b,c], Mahdi Ghorbani-Asl [a], Jannik C. Meyer [b,c], Arkady V. Krasheninnikov [a,*]

[a] Institute of Ion Beam Physics and Materials Research, Helmholtz-Zentrum Dresden-Rossendorf, Dresden, 01328, Germany
[b] University of Tübingen, Institute of Applied Physics, Tübingen, 72076, Germany
[c] NMI Natural and Medical Sciences Institute at the University of Tübingen, Reutlingen, 72770, Germany

ARTICLE INFO

Keywords:
Graphene nanopores
Strain engineering
DFT calculations
Midgap states
Antidot lattices
Vacancy defects
Magnetism

ABSTRACT

Creating a graphene nanomesh, that is graphene sheet with a regular array of holes, which can also be referred to as antidot lattice, is one of the ways to open the electronic band gap in graphene. Using focused electron irradiation in a transmission electron microscope and programmed beam displacements, we prepare nanomeshes with periodicities below 10 nm and hole sizes below 3 nm. We find that the formation of the mesh is frequently accompanied by the appearance of vacancy lines, which should give rise to the mechanical strain in the system. Moreover, strain can also appear upon heating or cooling graphene sheet along with the supporting frame, or exerted externally. At the same time, the effects of strain on the electronic structure of graphene nanomeshes has not been studied. The main goal of this work is to investigate theoretically how tensile strain and vacancy lines can affect the band gap in the nanomeshes with and without hydrogen termination. Using first-principles calculations, we demonstrate that for most structures the gap (if present) monotonously decreases with strain. However, when strain gives rise to the changes in the morphology of the edges, the gap can be opened or closed, which is associated with the spatial localization of the electron wave functions at the valence band maximum and conduction band minima. The magnetic moments localized at the edge atoms of the nanopore change as well. We further discuss such a behavior in the context of the optoelectronic properties of graphene antidot lattices, along with the implications for strain engineering of the characteristics of the nanomeshes.

1. Introduction

Graphene, a two-dimensional (2D) material which has been at the forefront of research in physics and materials science since its isolation in 2004 [1], possesses many unique properties such as record-high Young's modulus, excellent electron mobility and thermal conductance, just to mention a few [2]. However, pristine graphene has no electronic band gap, which limits its applications in electronics [3,4], photovoltaics [5,6] and sensing [7,8]. Not surprisingly, various strategies to open the gap in graphene have been explored theoretically and experimentally, which include chemical functionalization [9–12], placing graphene on various substrates [13–18], application of electric field (in bilayer graphene) [19–22], creation of superlattices [23–25], patterning and nanostructuring [26]. Specifically, a sizable band gap of up to 4.7 eV can be created in monolayer graphene by attaching various chemical groups (OH, F, H) and essentially converting it to another material, that is graphene oxide [27,28], graphane [29,30] or C–F compound [31–33]. A smaller band gap (less than 0.3 eV) can be induced in graphene on specific substrates, e.g., Au (001) [18], or h-BN [16,34].

As for the nanostructuring, first-principles [35,36] and tight-binding [37] calculations showed that graphene ribbons exhibit gaps with the value being dependent on ribbon width and edge type due to quantum confinement. Experimental studies [38–44] confirmed this conjecture. In particular, scanning tunneling spectroscopy experiments have revealed a bandgap of up to 0.39 eV for H-terminated zigzag graphene nanoribbons [38]. Another study where scanning tunneling microscopy/spectroscopy (STM/STS) measurements were employed has reported a bandgap of 0.75 eV in the armchair graphene nanoribbons [39]. Sub-nanometer ribbons synthesized inside carbon nanotubes have exhibited a bandgap of 1.83 eV [45].

Calculations [46–52] also indicated that creating an array of regularly spaced nanopores (NPs) in graphene, which can be referred to as a mesh of antidots, can convert it from semimetal to semiconductor. The gap opening and its magnitude was shown to be dependent on NP sizes, their shapes, periodicity and separations, and it could reach

* Corresponding author.
E-mail addresses: jannik.meyer@uni-tuebingen.de (J.C. Meyer), a.krasheninnikov@hzdr.de (A.V. Krasheninnikov).

https://doi.org/10.1016/j.cartre.2025.100602
Received 2 December 2025; Received in revised form 8 December 2025; Accepted 9 December 2025
Available online 12 December 2025

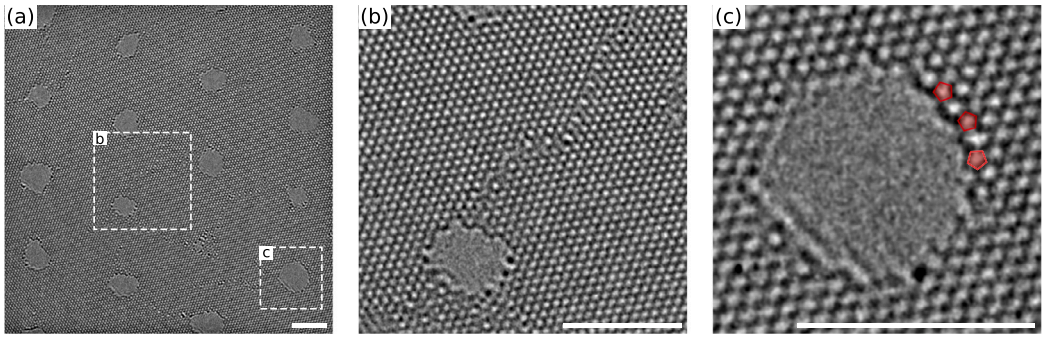

Fig. 1. (a) An example of the antidot lattice produced by the electron beam in the TEM at elevated temperatures. (b) Close up of a vacancy line near a nanopore in graphene, corresponding to the area b in panel (a). (c) Close up of the nanopore shown in panel (a), area c. Pentagons at the edge of the nanopore are clearly visible. Scale bars are 3 nm.

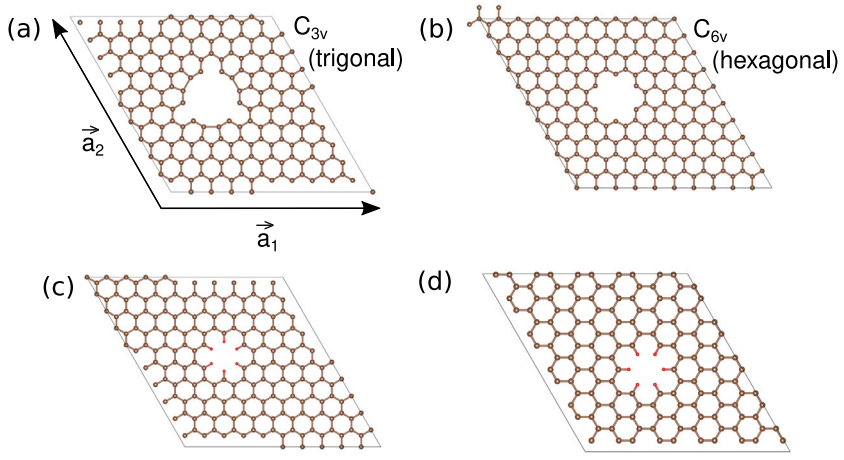

Fig. 2. (a) Example of a zigzag supercell with translation vectors $\vec{a}_1$ = (10,0), $\vec{a}_2$ = (10,0) expressed in terms of graphene unit vectors and a pore where 12 atoms are missing. (b–d) Examples of pores with various geometry and supercell sizes with and without hydrogen termination at the edges. Carbon atoms are colored brown and hydrogen atoms red.

several tenths of eVs for realistic structures. The influence of hydrogen passivation of the dangling bonds at the edges on the electronic structure was addressed as well [47]. The role of disorder at the edges was also investigated [53,54]. It was found that the gap is rather robust against geometrical disorder, and only a large deviation of the antidot array from the perfect periodicity leads to a narrowing and eventually closing of the energy gap.

Concurrently to the theoretical studies, a substantial progress in the manufacture of the antidot lattices was achieved [55]. The main fabrication methods for creating graphene NPs include electron beam milling, ion beam bombardment, plasma etching, electric breakdown, chemical treatments, photothermal effect-mediated etching and laser illumination, see Ref. [56] for an overview. In particular, nanomeshes were created in graphene on metal substrates using ion beam bombardment together with high-temperature annealing responsible for diffusion and agglomeration of irradiation-induced vacancies in specific areas of the moire pattern [57], but removal of the mesh from the substrate is not trivial due to the enhanced interaction of the substrate with the dangling bond atoms at the edges of the NPs. NPs with diameters ranging from 2 to 40 nm were produced by employing a focused electron beam in the transmission electron microscope (TEM) at an acceleration voltage of 300 kV [58,59]. Holes in bilayer graphene were also manufactured using this approach [60]. However, it was found that the electron irradiation carried out at room temperature can introduce undesired defects and artifacts, such as fast amorphization of the graphene crystal structure and carbon deposition, which may adversely affect the performance of the graphene nanomeshes.

At the same time, using electron beams at high temperatures in the in-situ TEM experiments can create clean, large area graphene antidot-lattices with very small spacing of 5 to 10 nm and hole sizes below 3 nm. The carbon atoms are sputtered by the electron beam [61–63] followed by vacancy diffusion and agglomeration as well as the reconstruction of the atomic lattice facilitated by elevated temperatures. An example is shown in Fig. 1. Besides the holes, vacancy lines which form partial dislocations are observed. Such defects are associated with local distortions of the lattice and hence indicate the presence of mechanical strain in the system [64].

Moreover, external strain can also be a way to tune the properties of a nanomesh if it can be applied in a controlled way. We note that although mechanical strain has widely been used to tune the electronic properties of 2D materials [65–67], application of strain to pristine graphene does not seem to open the gap, see Ref. [65] and references therein for the discussion. At the same time, strain created in the 2D material by the AFM tip [68], or its transfer to a special

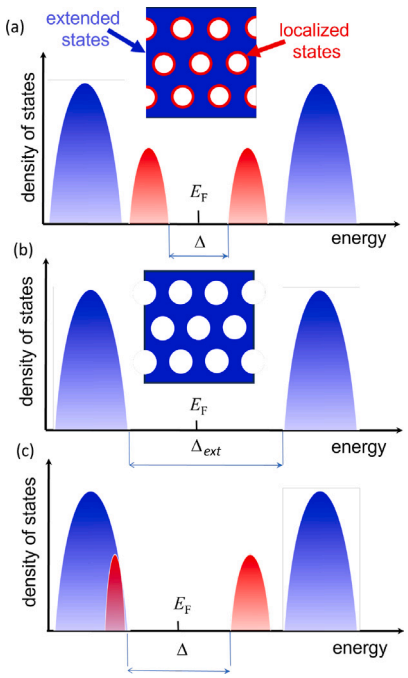

Fig. 3. Schematic diagram of the density of states of a graphene nanomesh illustrating the extended states at the valence band maximum and conduction band minimum and those localized at the holes. The states can be fully extended or at least one of the band edge states can be localized, in the former case we denote the gap Δ as Δ_{ext}.

substrate [69,70], its bending [71], or due to the presence of gas/water bubbles between sheets of the 2D material [72] can be used to tune the electronic structure of graphene nanomeshes. However, the effects of strain, external or due to the vacancy lines, on the characteristics of the nanomeshes with actual holes, not small vacancies [73], have not yet been addressed. The main goal of this paper is to theoretically study these issues. Using first-principles calculations, we systematically investigate the effects of tensile strain on the morphology and electronic structure of graphene nanomeshes with holes of various types, sizes and separations. We also study how vacancy lines influence the electronic structure of the antidot lattices.

2. Experimental and computational details

2.1. Experimental

The graphene meshes shown were formed by nano-patterning a graphene sheet in a JEOL ARM200F transmission electron microscope (TEM). The TEM was operated at 200 kV in the scanning-TEM mode for patterning and at 80 kV in the aberration-corrected TEM mode for imaging. The sample was kept at an elevated temperature (ca. 500 °C) during patterning and imaging to avoid contamination [74]. For patterning, a script was used to move the beam to points, placed in a nearly hexagonal pattern. The details of the manufacture process will be published elsewhere.

2.2. Calculation setup

Our spin-polarized density functional theory (DFT) calculations were carried out using generalized gradient approximation (GGA) with the Perdew–Burke–Ernzerhof parametrization [75] as implemented in the VASP code [76,77]. A plane-wave cut-off of 400 eV was used in all the calculations. Vacuum space of 16 Å was added for all systems in the directions perpendicular to the graphen planes to avoid the spurious inter-layer interactions. The full geometry and shape optimizations were performed with the force tolerance being set to 0.01 eV/Å. The Brillouin zone of the studied systems was sampled using a $9 \times 9 \times 1$ k-point mesh for the supercells. For accurate density of states (DOS) calculations we used the tetrahedron method [78–80]. The partial charge densities and spin difference densities were processed using, VESTA [81] and VASPKIT [82].

2.3. Different types of pore geometries

To assess the effects of strain on the electronic structure of graphene antidot lattices, we employed the supercell approach. As theoretically demonstrated in a number of papers [47,48,52], the appearance of the gap upon nanomesh creation depends on the shape of the NPs, their symmetry and unit vectors of the lattice. For example, if the supercell vectors are oriented along the zigzag directions of the underlying graphene lattice, then sizable gap is opened provided that vector length (expressed in terms of graphene unit vectors) is a multiple of three [52]. Likewise, for vectors oriented along armchair directions, the gap is open when the number of the zigzag chains oriented perpendicular the armchair direction is even [48]. As there is essentially an infinite number of possible configurations, we pick up several representative systems composed from pores of various radii and separations between them with and without gap when there is no strain.

Following previous work [46,47,52,83–85], we use general notations $(\vec{a}_1, \vec{a}_2)$ to describe the periodic supercells by their translation vectors $\vec{a}_1$ and $\vec{a}_2$, which are expressed in terms of the graphene unit vectors and lattice constant of $a = 2.46$ Å . We also indicate the number of removed atoms, the symmetry of the pore and the types of the edges, which can be either zigzag or armchair. We note that after the optimization the average lattice constant calculated as the ratio of the supercell size to the number of primitive cells was different from that in pristine graphene, but the difference was less than 2%, specific for each system. The changes in the angles were less than 2 degrees. The systems we studied are summarized in Table 1.

3. Results and discussion

3.1. Graphene nanomeshes created using the electron beam

The pattern shown in Fig. 1(a) represents a hexagonal nanomesh with a spacing of ca. 8 nm between the centers of NPs. At each point the beam was parked for 2.5 s to make a hole in graphene. Some distortions in the lattice occur due to sample drift during patterning. The exposure to the electron beam associated with the sputtering of C atoms [61] and migration/agglomeration of vacancies at elevated temperatures gave rise to the formation of not only NPs, but also vacancy lines, Fig. 1(b), which may give rise to the intrinsic tensile strain in the system. We note that the reconstruction of the edges gives rise to the formation of pentagons, as illustrated in Fig. 1(c).

3.2. Simulated pores with various morphologies

Fig. 2(a) presents an example of a unit cell and Fig. 2(b–d) shows pores with different geometries, which have been fully optimized. We studied the naked edges and those passivated with H atoms. The naked edges can reconstruct [86] by saturating some of the dangling bonds and forming pentagons, as evident from Fig. 2(a). We stress that although under ambient conditions edges are expected to be passivated, they can remain naked in the in situ TEM experiments carried out in ultra-high vacuum, as H atoms can easily be sputtered away.

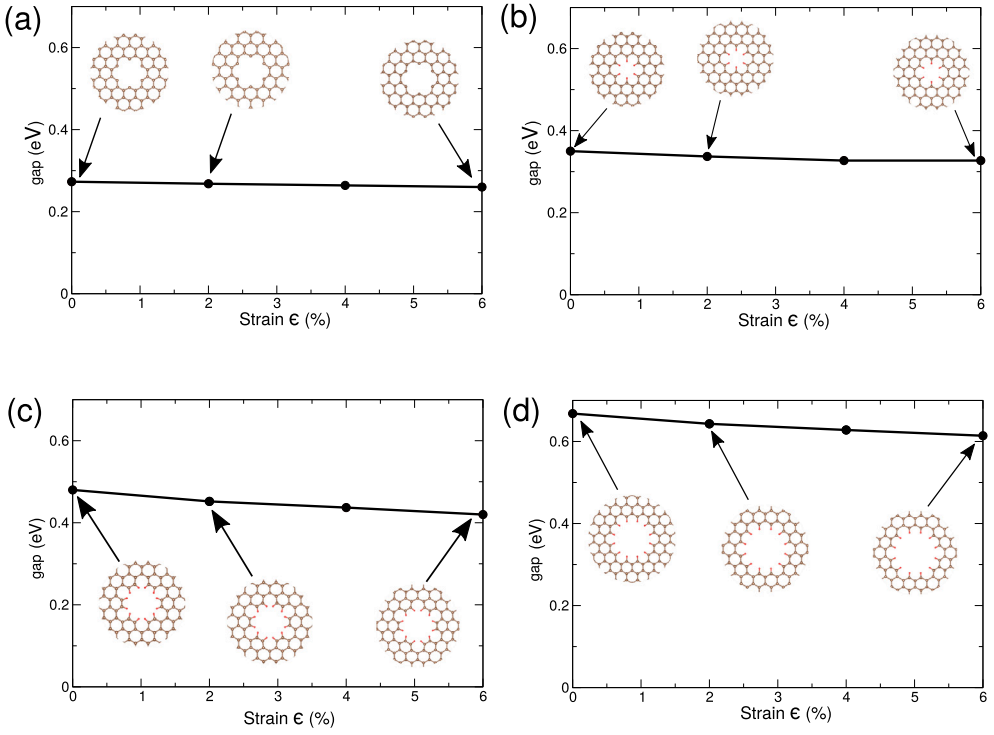

Fig. 4. Dependence of the electronic gap on tensile bi-axial strain for several nanomeshes. (a) nanomesh with 6 atoms missing in a 9 × 9 zigzag supercell. (b) Nanomesh with 6 atoms missing in a 9 × 9 zigzag supercell, where the dangling bonds at the pore edges are passivated with H atoms. (c) Nanomesh with 12 atoms missing in a 9× 9 zigzag supercell, where the dangling bonds at the pore edges are passivated with H atoms. (d) Nanomesh with 24 atoms missing in a 9 × 9 zigzag supercell, where the dangling bonds at the pore edges are passivated with H atoms.

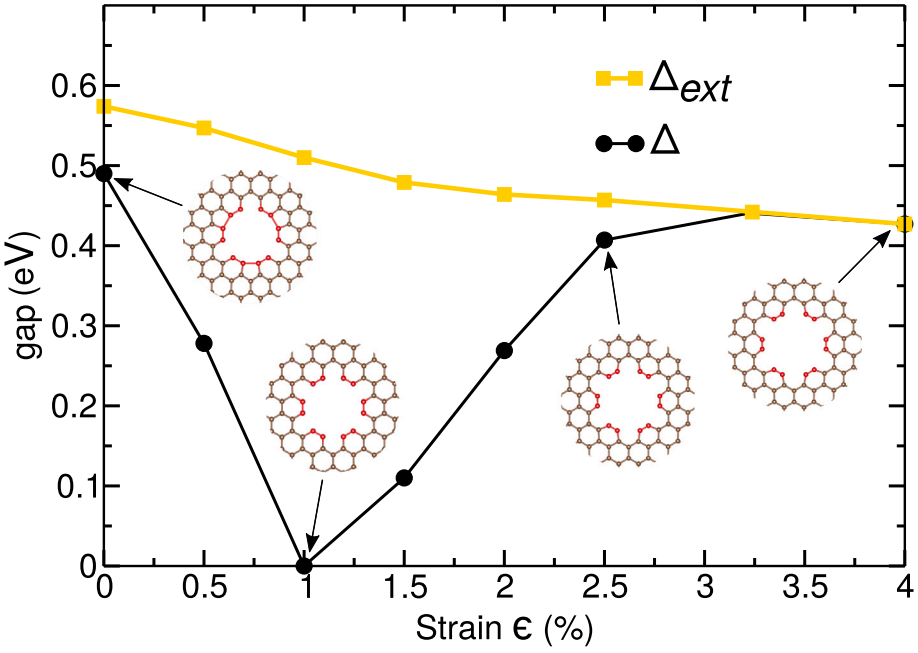

Fig. 5. Dependence of the electronic gap Δ and the gap formed by extended states Δ_{ext} on tensile bi-axial strain for nanomesh with 12 atoms missing in a 9 × 9 zigzag supercell. The carbon atoms at the edges are colored red.

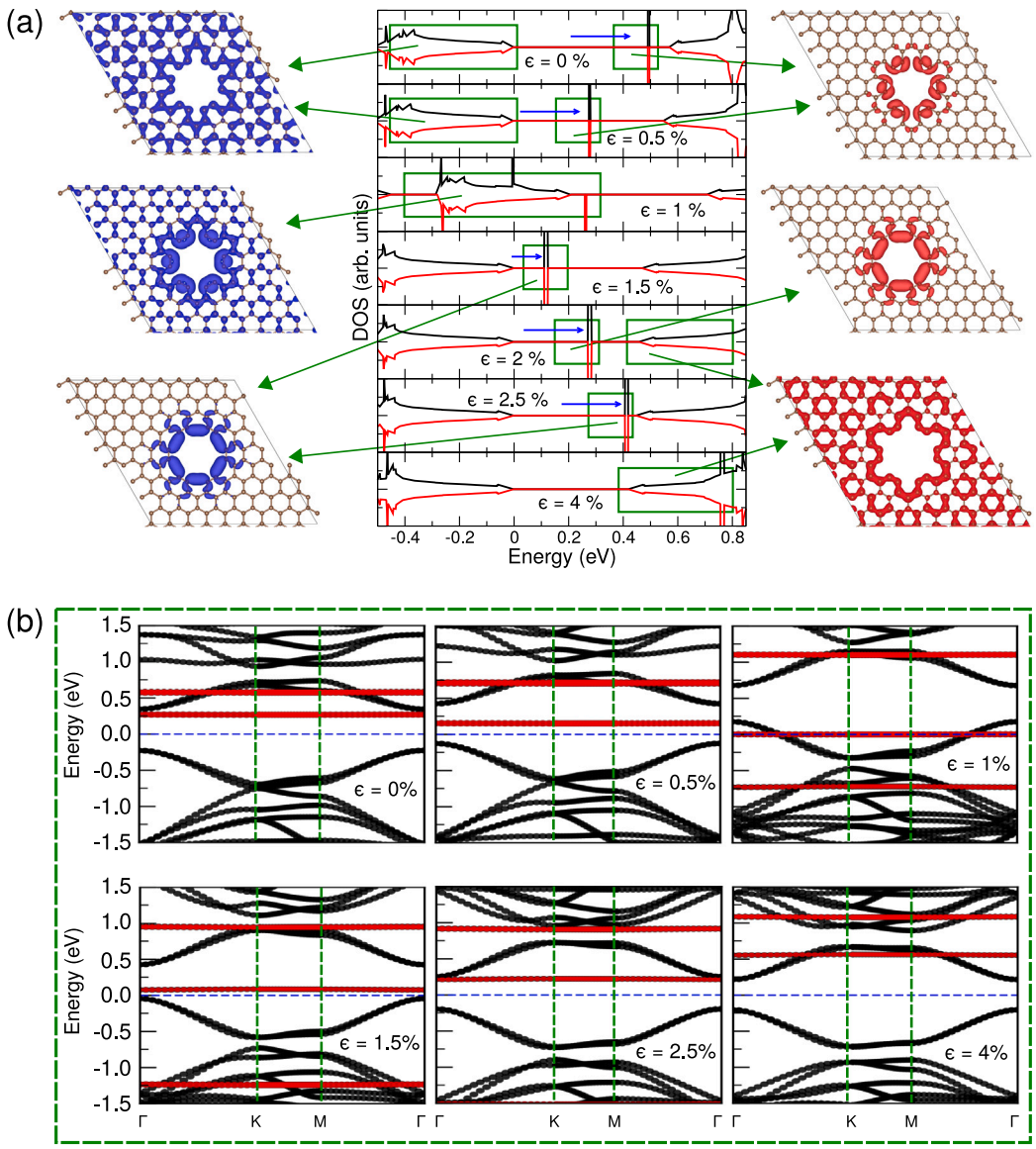

Fig. 6. (a) Density of states (DOS) along with the spatial distribution of the partial electron density associated with the specific states and (b) the band structures for different strain values ϵ for nanomesh with 12 atoms missing in a 9 × 9 zigzag supercell. Flat bands colored red correspond to the states localized at the edges of the nanopore, as illustrated in the insets in Fig. 5. The isosurface was set to 0.002 eÅ^{-3} for the partial charge.

3.3. Electronic structure of the graphene nanomeshes without strain

The effects of periodic arrays of holes on the electronic structure of graphene can be straightforwardly assessed from the changes in the electronic density of states (DOS). To establish a connection with the previous theoretical work, we first calculated the electronic structure of the nanomesh without strain, and obtained results, which are very close to the published results, see Table 1. Obviously the bandgap Δ depends on the geometries of the pores and their separation, as reported previously. We note that DFT with semilocal exchange–correlation functionals is known to underestimate the band gap [87], so that the band gaps in the experimentally manufactured structures may be larger as the calculations predict.

An important point is the character of the states at the valence band maximum (VBM) and conduction band minimum (CBM). The states can be localized at the holes or be of an extended character, as schematically illustrated in Fig. 3(a,b). It is also possible that VBM states are delocalized, while the CBM states are localized, Fig. 3(c). To emphasize that both CBM and VBM states are fully extended, we use notation Δ_{ext}, and in this case $\Delta = \Delta_{ext}$.

3.4. Effects of strain on the electronic structure of graphene nanomeshes

To understand the effects of strain on the electronic structure of graphene nanomeshes, we applied biaxial tensile strain (up to 6%) to the system by increasing the supercell size. We did not consider compressive strain, as thin and flexible 2D material like graphene would rather buckle and develop ripples upon compression. We studied first nanomeshes with fully passivated edges of the pores, e.g., nanomesh with 6 atoms missing in a 9 × 9 zigzag supercell, nanomesh with 12 atoms missing in a 9 × 9 zigzag supercell, and that with 24 atoms missing in a 9 × 9 zigzag supercell. Our calculations indicate that for all the systems the gap linearly decreases with strain, as illustrated in Fig. 4. This is in-line with the general behavior of the gap in the

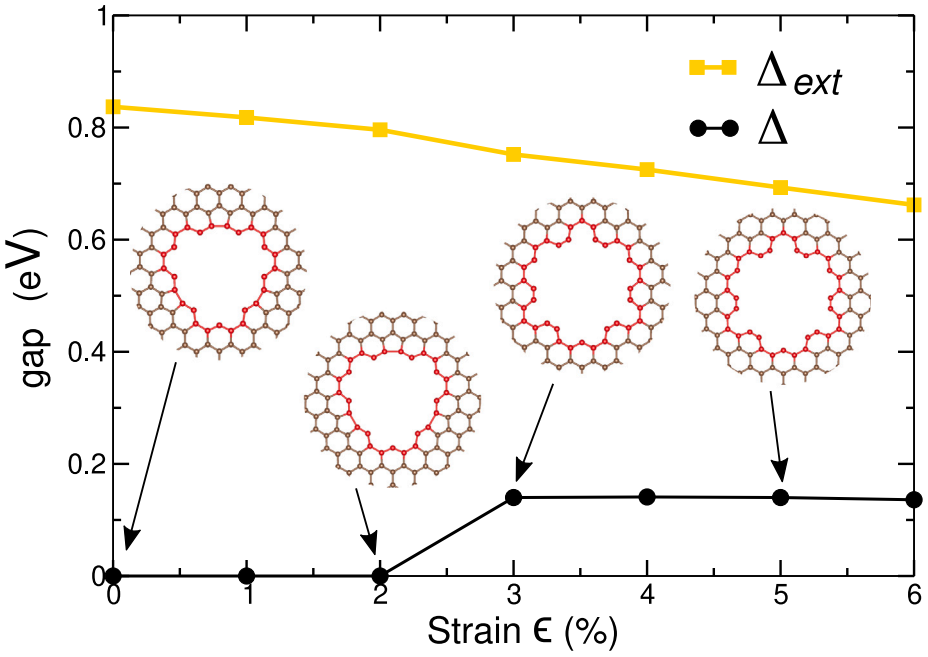

Fig. 7. Dependence of the electronic gap Δ and the gap formed by extended states Δ_{ext} on tensile bi-axial strain for the nanomesh with 25 atoms missing in a 10 × 10 zigzag supercell. The carbon atoms at the edges are colored red.

majority of semiconductors upon strain where tensile strain increases atom separation and gives rise to a smaller energy difference between the conduction band minimum and valence band maximum, which can be associated with the splitting of the atomic levels upon formation of the compound [65,88,89], or in the simplest case in a dimer. We note that no noticeable structural changes at the hole edges occur. The analysis of the electronic structure indicated that the VBM and CBM are formed by the extended states, or those strongly hybridized with the states localized at the edges of the NPs.

However, the situation is much more interesting when there are states close to the Fermi energy localized at the edges of the NPs, and the atomic configuration of the edges and the symmetry of the NP change upon strain. As shown previously by Fürst et al. [90], sublattice imbalance leads to the occurrence of low-dispersion midgap bands in graphene nanopore systems. An example of such transformations is the break-up of the C–C bonds at pentagons, as illustrated in the inset in Figs. 5 and 6. Moreover, the analysis of the behavior of the states at the band edges, Fig. 6(a) indicates that Δ and Δ_{ext} are different in this case, as the localized states move across the band gap formed by the delocalized states, so that the gap formally first decreases and vanishes at 1% strain, then appears again. The overlap of extended and localized states is clearly observable in the partial (corresponding to narrow energy ranges) charge distribution in the real space. The changes in the electronic structure are also evident from Fig. 6(b), where the flat bands associated with the states localized at the pore edges are indicated in red, along with the edge atoms at the edges of the NP. It is evident from Figs. 5 and 6 that, at strain $\epsilon = 1\%$ the bonds at pentagons break, which gives rise to the change in the electronic structure and gap re-opening. We note that the change in the morphology of the edges is accompanied by the change in the symmetry of the pore from trigonal (C_{3v}) to hexagonal (C_{6v}). Such changes in the electronic structure should affect electronic transport and optoelectronic properties of the nanomesh.

We studied also the graphene nanomesh system with 25 atoms missing in a 10 × 10 zigzag supercell, Figs. 7 and 8(a). The edges include pentagons, analogously to the case with 12 missing atoms considered above. Without any strain the system has sublattice imbalance which leads to emergence of flat bands, but here the gap is 0 eV. When biaxial tensile strain is applied, after $\epsilon = 2\%$ the bonds at the pentagons break, and a gap of 0.15 eV opens. We note that when only extended states are considered, the gap Δ_{ext} decreases.

To get further insights into the effects of edge reconstructions on the electronic characteristics, we investigated another nanomesh having pores with 16 atoms missing in a 9 × 9 zigzag supercell, Figs. 9 and 10. If $\epsilon = 0\%$ the system does not possess bandgap. However, when $\epsilon > 1\%$ is applied, the bonds at the pentagons break and a finite bandgap of 0.22 eV is opening. So, in the systems illustrated in Figs. 7 and 9 a semimetal to semiconductor transition takes place because of the influence of the external tensile strain.

The changes in the electronic structure of the nanomeshes upon strain with various supercell sizes, pore geometries and pore symmetries are summarized in Table 1. The green rows represent NP systems where the bandgap remains roughly the same or decreases, the yellow rows stands for the nanopore systems where the bandgap either changes from 0 eV to a finite value or the vice versa and the red row corresponds to the system where there is an interplay between localized/delocalized states and non-trivial changes in the electronic structure.

Previously it has been shown that for specific NP geometries there is a total non-zero magnetization in the nanomesh [91,92]. To address the effects of strain on the magnetic properties of the nanomeshes we calculated the total magnetization of the system and also magnetic moments localized at the pore edge atoms with dangling bonds. We studied the changes in magnetic characteristics for several nanomeshes, and found that the dependence of magnetization on strain is not trivial. As an example, below we present the results for the 10 × 10 zigzag supercell with 25 atoms missing and another one with 16 atoms missing in a 9 × 9 zigzag supercell. When external biaxial tensile strain ϵ is applied, Fig. 11(a,b) the magnetic moments localized at the edges are changing, along with the total magnetization. In particular, for graphene NP with 25 atoms missing in a 10 × 10 zigzag supercell the magnetization decreased from $9.5\mu_B$ to $4\mu_B$. Such a behavior is related to bond breaking, as evident from Fig. 11(a). At strain values

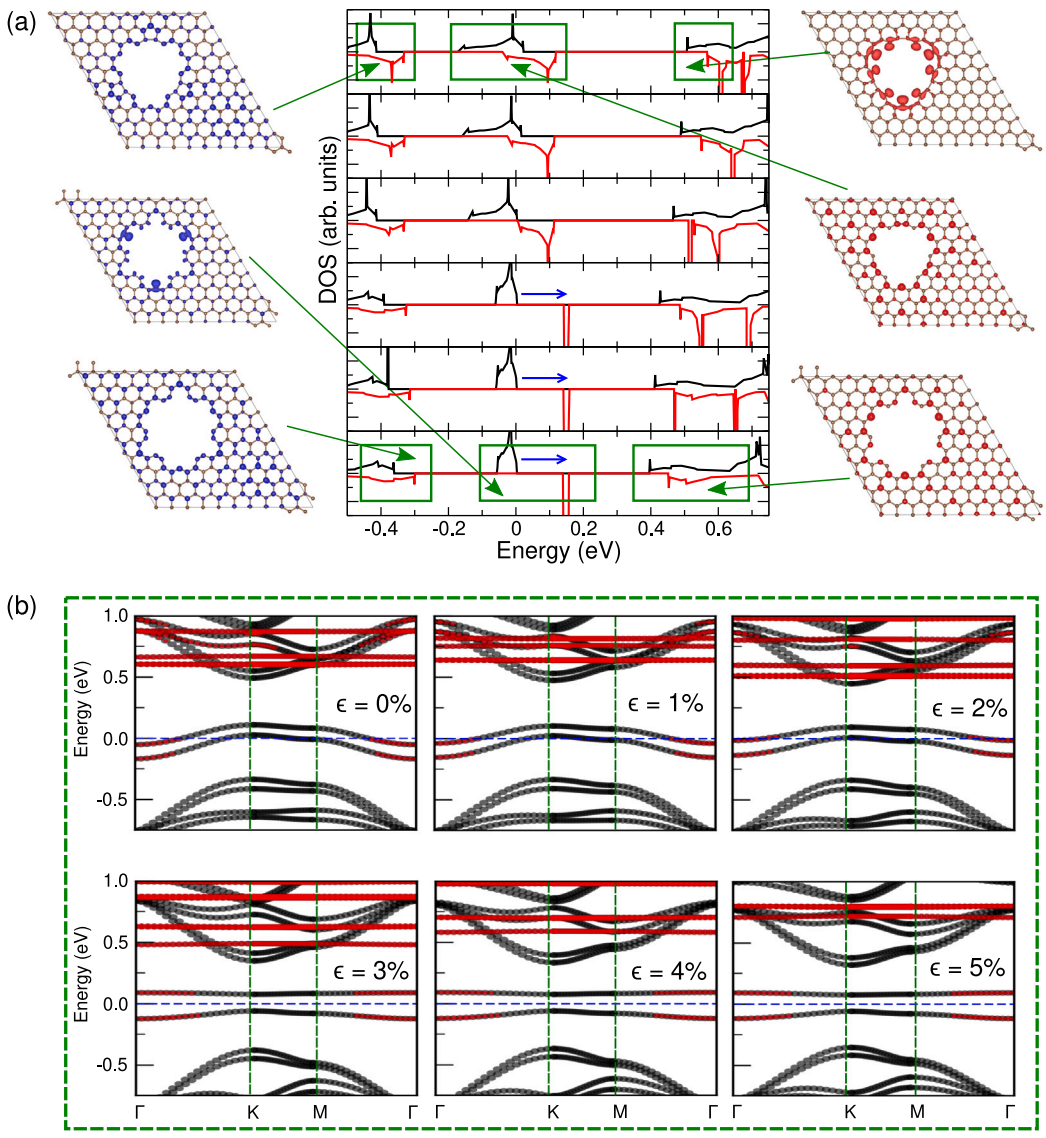

Fig. 8. (a) Density of states (DOS) and (b) the band structures for different strain values ϵ for the nanomesh with 25 atoms missing in a 10 × 10 zigzag supercell. At ϵ above 2% a gap is opened. The isosurface was set too 0.002 eÅ^{-3} for the partial charge. Flat bands colored red correspond to the states localized at the edges of the nanopore, as illustrated in the insets in Fig. 7.

around ϵ = 2%, some of the bonds at the NP edges break and other bonds get reorganized. Pairs of C atoms in the armchair configuration appear, which apparently do not have magnetic moments, as they are on different sublattices in graphene. At the same time, for the triangular NP with 16 atoms missing in a 9 × 9 zigzag supercell, Fig. 11(b), the magnetization increases with strain and jumps up at $\epsilon \sim 1.5\%$ when bonds at pentagons in the corners of the pore break and larger magnetic moments appear on atoms in the same sublattice [93]. Overall, the changes in magnetization can be attributed to bond breaking and geometry changes at the edges of the pores.

3.5. Mesh with vacancy lines

As in the experiment the exposure of the system to electron irradiation at elevated temperatures resulted in the formation of not only pores, but also vacancy lines, we also studied how the lines can affect the electronic structure of the system. Moreover, as discussed above, vacancy lines themselves can give rise to the development of tensile strain in the suspended graphene sheet partly clamped to the substrate (or TEM grid) outside the mesh area. The lines appear in the zigzag directions by forming 55-8 rings or in the armchair direction consisting of 4-8 rings. The examples of graphene structures with pores, lines and combined pore-line systems are presented in Fig. 12.

The effects of the vacancy lines on the electronic, magnetic and mechanical properties of graphene have been studied at length before [94–98]. It has been shown that both the 55-8, Fig. 12(a), and 4-8, Fig. 12(e), vacancy lines give rise to new states close to the Fermi level making the system essentially metallic. Our calculations also indicated that, see Fig. 12(d,h), where the DOS of the graphene sheets with line defects is presented in green.

To understand how vacancy lines alter the electronic structure of the nanomesh, we chose rectangular supercells with nanopores exhibiting gaps, Fig. 12(b,f) and constructed the combined systems, Fig. 12(c,g). As evident from our calculations, the 55-8 line defect preserves the gap in the system, although its value decreases from 0.1 to 0.07 eV. At the same time, the 4-8 vacancy line made the system fully metallic.

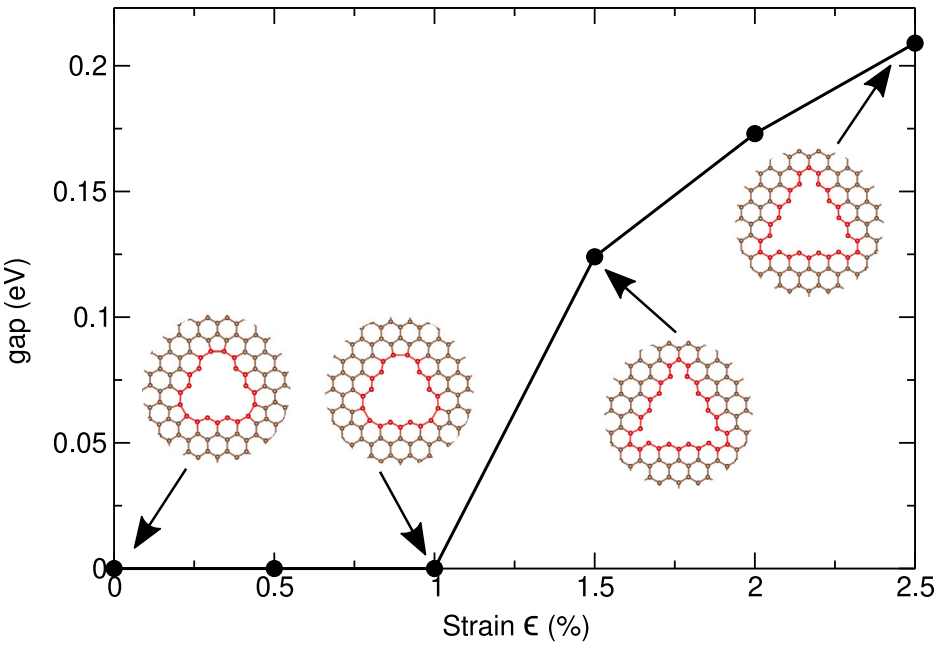

Fig. 9. Dependence of the gap on tensile bi-axial strain for nanomesh with 16 atoms missing in a 9 × 9 zigzag supercell. The carbon atoms at the edges are colored red.

Table 1
Electronic structure (bandgap in eV) of different nanopore systems in graphene containing different edges, symmetries, geometry and hydrogen passivation with strain ϵ. The last two columns present the values of the band gap obtained in our calculations.

System	Unit vectors	Missing atoms	w/out H	Symmetry	Geometry	gap	Gap $\epsilon = 0\%$	Gap $\epsilon = 3\%, 6\%$
Zigzag	9 × 9	6	Yes	C_{6v}	hex	0.45 [84]	0.35	0.33, 0.32
Zigzag	9 × 9	6	No	C_{6v}	hex	–	0.30	0.29, 0.28
Zigzag	10 × 10	6	Yes	C_{6v}	hex	0.00 [84]	0.00	0.00, 0.00
Zigzag	10 × 10	6	No	C_{6v}	hex	–	0.00	0.00, 0.00
Zigzag	9 × 9	12	Yes	C_{6v}	hex	–	0.48	0.45,0.42
Zigzag	9 × 9	12	No	$C_{3v} \rightarrow C_{6v}$	triang→hex	0.60 [52]	0.58	0.47, 0.40
Zigzag	10 × 10	12	Yes	C_{6v}	hex	–	0.00	0.00, 0.00
Zigzag	10 × 10	12	No	$C_{3v} \rightarrow C_{6v}$	triang→hex	0.00 [52]	0.11	0.00, 0.00
Zigzag	9 × 9	16	No	C_{3v}	triang	–	0.00	0.22, 0.22
Zigzag	9 × 9	24	Yes	C_{6v}	hex	0.65 [52]	0.66	0.64, 0.62
Zigzag	9 × 9	24	No	C_{6v}	hex	0.60 [52]	0.52	0.50, 0.49
Zigzag	10 × 10	24	Yes	C_{6v}	hex	0.00 [52]	0.00	0.00, 0.00
Zigzag	10 × 10	24	No	C_{6v}	hex	0.20 [52]	0.15	0.14, 0.13
Zigzag	10 × 10	25	yes	C_{3v}	triang	–	0.10	0.10, 0.10
Zigzag	10 × 10	25	No	C_{3v}	triang	–	0.00	0.15, 0.15
Armchair	5 × 5	6	Yes	C_{6v}	hex	0.40 [48]	0.37	0.37, 0.36
Armchair	5 × 5	6	No	C_{6v}	hex	–	0.30	0.30, 0.29
Mixed	3 × 7	6	Yes	C_{6v}	hex	0.00 [84]	0.00	0.00, 0.00
Mixed	3 × 7	6	No	C_{6v}	hex	–	0.00	0.00, 0.00

In the above calculation the structure is periodic in all directions, so that vacancy lines extend across the whole system, constituting an infinite network of holes and lines. As vacancy lines may connect only two specific holes, we also studied the case when two holes are connected by the 55-8 line, Fig. 13. As zigzag chain of C atoms must be removed from the structure to make the line, this obviously created lots of internal strain, which was partly removed by out-of-plane relaxation, Fig. 13(a,b). We note that although the supercell size was relaxed, the supercell consisting of 428 atoms is not large enough to match the experiment, which exaggerated the deformation. However, our results indicate that some out-of-plane deformation is also likely present in the real experimental structures. DOS calculations showed that the system is metallic, Fig. 13(c), with the stated close to the Fermi level being localized on vacancy lines. Overall, our results indicate that vacancy lines can provide conducting channels between holes representing antidots potentially rendering interesting interplay between electronic states localized at the edges of the pores and extended states at the vacancy lines.

4. Conclusions

Our experimental results provide evidence that nano-patterning of graphene in a transmission electron microscope makes it possible to create nano-meshes with periodicities below 10 nm by sputtering carbon

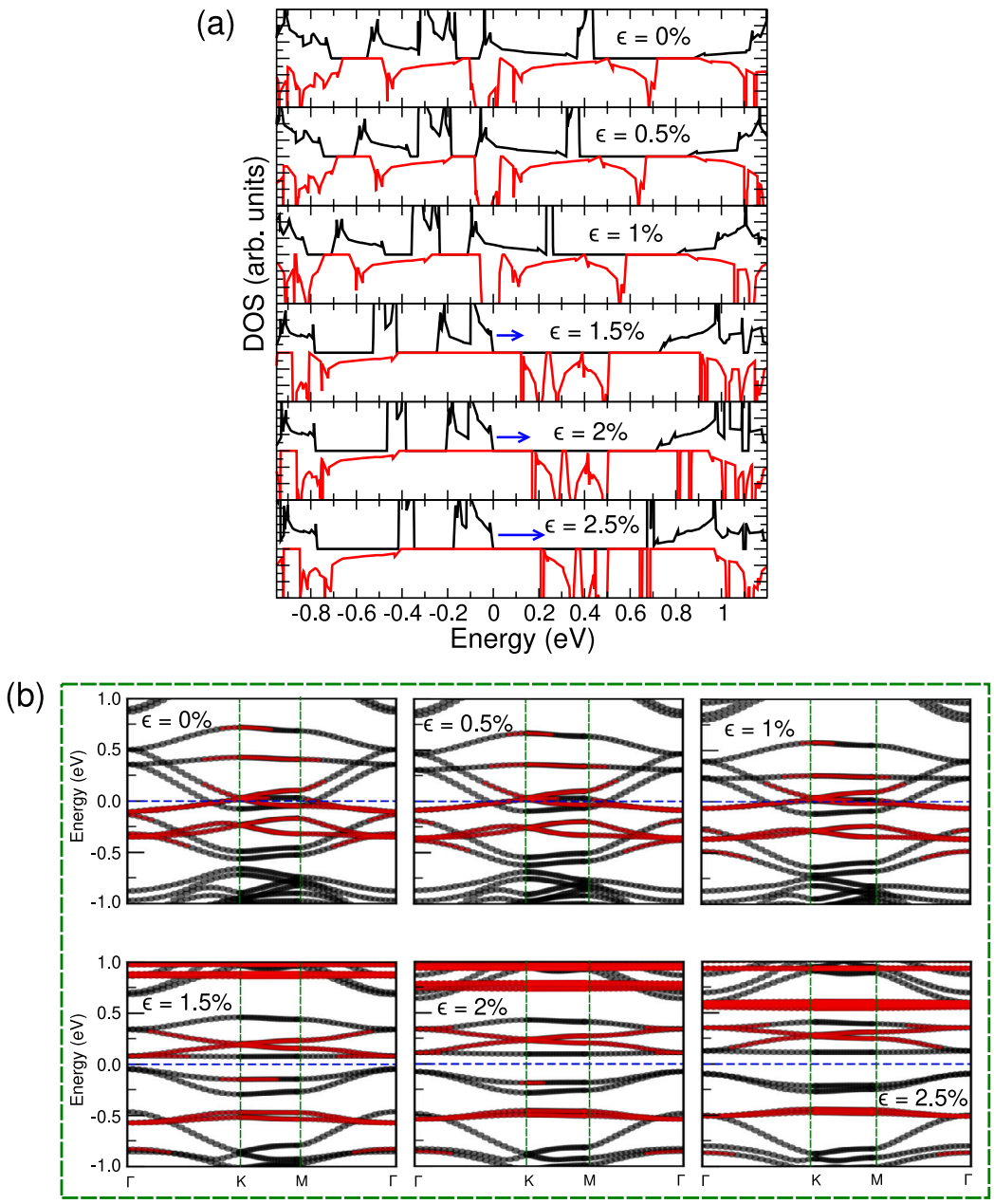

Fig. 10. (a) Density of states (DOS) along with the spatial distribution of the partial electron density associated with the specific states for different external biaxial tensile strain ϵ and (b) dependence of the bandstructure on tensile bi-axial strain. At $\epsilon = 1\%$ the gap is opening. The bands colored red represents projection on the atoms at the edges of the nanopore.

atoms in pre-selected areas. Heating the graphene during sputtering helps to avoid contamination buildup under the beam, but it also stimulates vacancy diffusion and agglomeration into NPs and vacancy lines. As a result, the area between the NPs is free from point defects. However, the partial dislocations formed by the vacancy lines are a clear indication of strain, which is relaxed to some extent by these configurations. Our first-principles calculations indicate that for most graphene nanomeshes the gap (if present) monotonously decreases with strain. However, when tensile strain gives rise to the changes in the morphology of the edges, the gap can be opened or closed, which is associated with the extension/delocalization of the electron wave functions at the valence band maximum and conduction band minimum.

The changes in the electronic structure of nanomeshes and in magnetic moments upon strain predicted by the calculations should be experimentally measurable, as they affect optical and magnetic properties as well as the electronic transport in the system. This suggests that the characteristics of graphene nanomeshes can further be engineered by external strain and as the gap opening under strain is a reversible process, such systems could potentially be used as strain sensors. At the same time, the dependence of the local magnetic moments on strain indicates that these systems can also be used as magnetic sensors or spintronic devices. Moreover, because of the specially localized character of the magnetic moments, these pores can be coupled with other magnetic entities like molecules, different atoms, clusters of atoms and 2D materials in a heterostructure, which can give rise to new physical

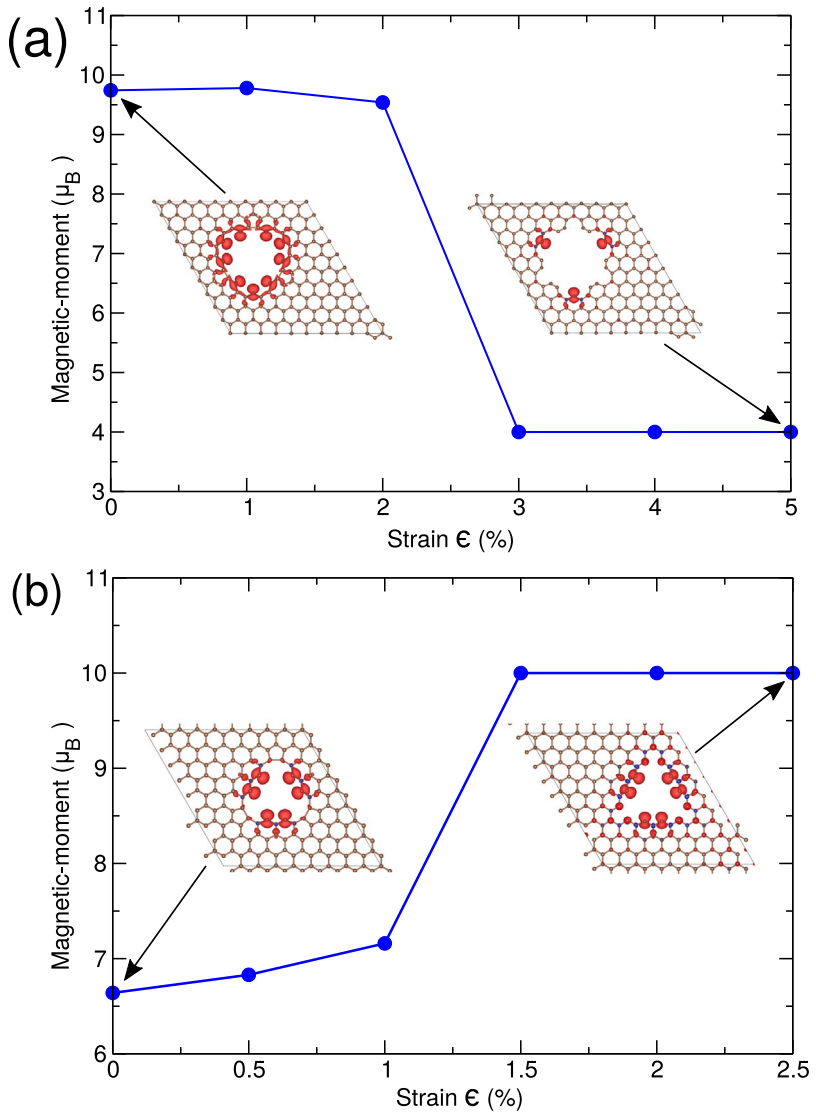

Fig. 11. Dependence of magnetic-moments on biaxial tensile strain for graphene nanopore with 25 atoms missing in a 10 × 10 zigzag supercell (a) and graphene nanopore with 16 atoms missing in a 9 × 9 zigzag supercell (b). The insets show spin density for the zero and maximum values of strain. The isosurface was set to 0.005 eÅ^{-3} for the spin density.

properties combining magnetism, optics and electronics.

CRediT authorship contribution statement

Prosun Santra: Writing – original draft, Investigation, Data curation. **Michael Schlegel:** Writing – review & editing, Methodology, Investigation. **Mahdi Ghorbani-Asl:** Writing – review & editing, Validation, Investigation, Formal analysis. **Jannik C. Meyer:** Supervision, Project administration, Funding acquisition, Formal analysis, Conceptualization. **Arkady V. Krasheninnikov:** Writing – review & editing, Validation, Supervision, Project administration, Funding acquisition, Conceptualization.

Declaration of competing interest

The authors declare the following financial interests/personal relationships which may be considered as potential competing interests: Arkady Krasheninnikov reports financial support was provided by German Research Foundation. Jannik Meyer reports financial support was provided by German Research Foundation. If there are other authors, they declare that they have no known competing financial interests or personal relationships that could have appeared to influence the work reported in this paper.

Acknowledgments

We acknowledge funding from the German Research Foundation (DFG), project KR 4866/9-1 and ME3313/6-1, as well as the collaborative research center "Chemistry of Synthetic 2D Materials" CRC-1415-417590517. Generous CPU time grants from the Paderborn Center for Parallel Computing (PC2, Noctua 2 cluster, hpc-prf-def2dhet) and Gauss Centre for Supercomputing e.V. (http://www.gauss-centre.eu), Supercomputer HAWK at Höchstleistungsrechenzentrum Stuttgart, are greatly appreciated.

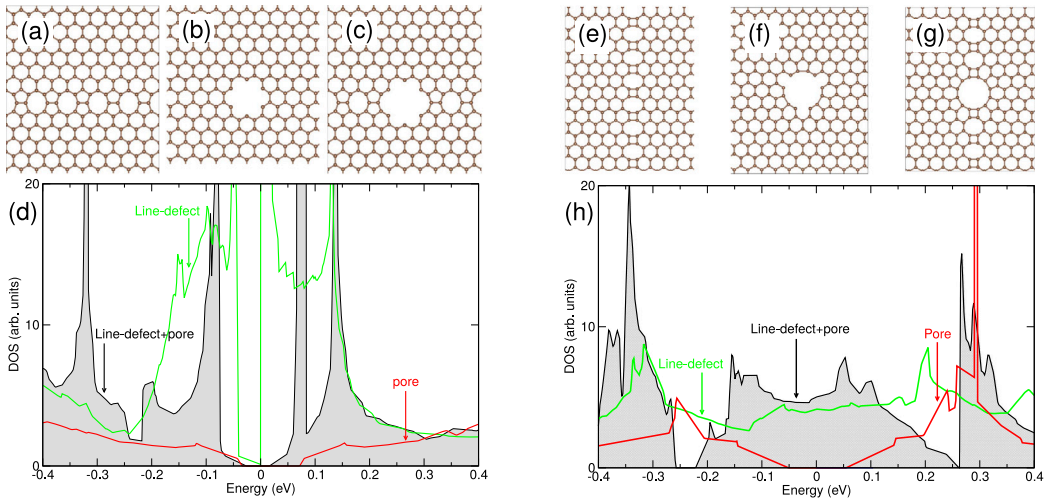

Fig. 12. Fully optimized atomic structures of (a) 55-8 vacancy line, (b) nanomesh with 6 atoms missing in a 10 × 6 mixed-edge rectangular supercell, and (c) 55-8 line defect with pore and (d) DOS for the above mentioned structures. Fully optimized atomic structures of (a) 4-8 vacancy line, (b) nanomesh with 12 atoms missing in a 10 × 7 mixed-edge rectangular supercell, and (c) 4-8 line defect with pore and (d) DOS for the above mentioned structures.

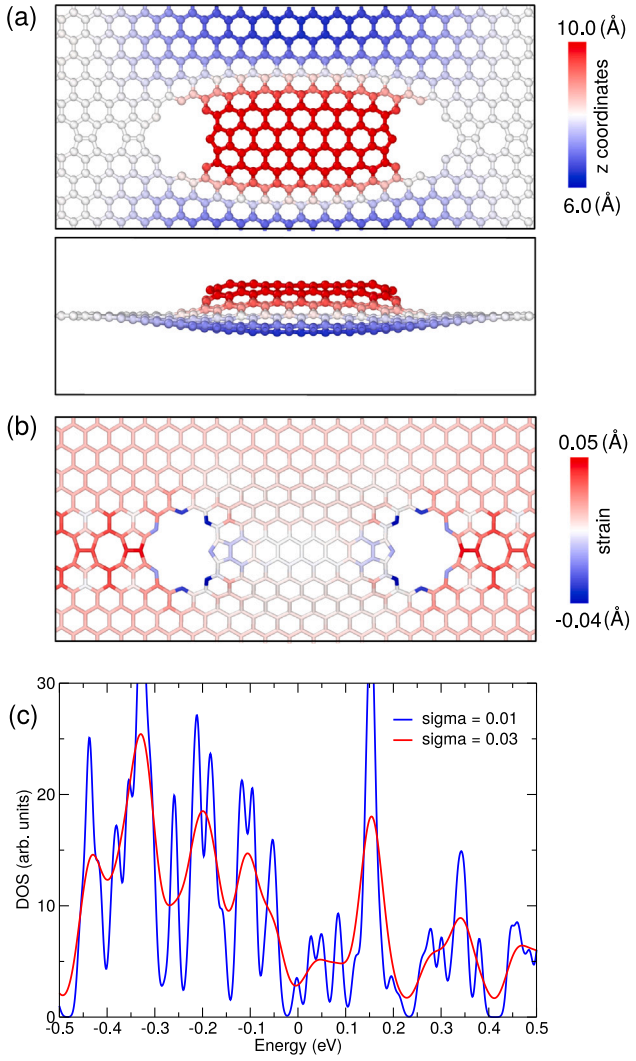

Fig. 13. Fully optimized structure of the a 55-8 vacancy line connecting two pores, top view (a) and side view (b). The atoms are colored according to their z−coordinate. (c) The total DOS of the system. Zero energy corresponds to the Fermi level.

Data availability

Data will be made available on request.

References

[1] K.S. Novoselov, A.K. Geim, S.V. Morozov, D. Jiang, Y. Zhang, S.V. Dubonos, I.V. Grigorieva, A.A. Firsov, Electric field effect in atomically thin carbon films, Science 306 (2004) 666–669, http://dx.doi.org/10.1126/science.1102896.

[2] A.K. Geim, K.S. Novoselov, The rise of graphene, Nat. Mater. 6 (2007) 183–191, http://dx.doi.org/10.1038/nmat1849.

[3] J.M. Marmolejo-Tejada, J. Velasco-Medina, Review on graphene nanoribbon devices for logic applications, Microelectron. J. 48 (2016) 18–38, http://dx.doi.org/10.1016/j.mejo.2015.11.006.

[4] J. Trasobares, J.C. Martín-Romano, M.W. Khaliq, S. Ruiz-Gómez, M. Foerster, M.Á. Niño, P. Pedraz, Y.J. Dappe, M.C. de Ory, J. García-Pérez, M. Acebrón, M.R. Osorio, M.T. Magaz, A. Gomez, R. Miranda, D. Granados, Hybrid molecular graphene transistor as an operando and optoelectronic platform, Nat. Commun. 14 (1) (2023) 1381, http://dx.doi.org/10.1038/s41467-023-36714-7.

[5] J.-K. Chang, Y.-Y. Huang, D.-L. Lin, J.-I. Tau, T.-H. Chen, M.-H. Chen, Solution-processed, semitransparent organic photovoltaics integrated with solution-doped graphene electrodes, Sci. Rep. 10 (1) (2020) 20010, http://dx.doi.org/10.1038/s41598-020-77012-2.

[6] P. Jain, R.S. Rajput, S. Kumar, A. Sharma, A. Jain, B.J. Bora, P. Sharma, R. Kumar, M. Shahid, A.A. Rajhi, M. Alsubih, M.A. Shah, A. Bhowmik, Recent advances in graphene-enabled materials for photovoltaic applications: A comprehensive review, ACS Omega 9 (11) (2024) 12403–12425, http://dx.doi.org/10.1021/acsomega.3c07994.

[7] A. Maity, H. Pu, X. Sui, J. Chang, K.J. Bottum, B. Jin, G. Zhou, Y. Wang, G. Lu, J. Chen, Scalable graphene sensor array for real-time toxins monitoring in flowing water, Nat. Commun. 14 (1) (2023) 4184, http://dx.doi.org/10.1038/s41467-023-39701-0.

[8] D. Shahdeo, A. Roberts, N. Abbineni, S. Gandhi, Chapter eight - graphene based sensors, in: C.M. Hussain (Ed.), Analytical Applications of Graphene for Comprehensive Analytical Chemistry, in: Comprehensive Analytical Chemistry, vol. 91, Elsevier, 2020, pp. 175–199, http://dx.doi.org/10.1016/bs.coac.2020.08.007.

[9] D.W. Boukhvalov, M.I. Katsnelson, Tuning the gap in bilayer graphene using chemical functionalization: Density functional calculations, Phys. Rev. B 78 (2008) 085413, http://dx.doi.org/10.1103/PhysRevB.78.085413.

[10] S.-F. Wang, L.-Y. Chen, J.-M. Zhang, Significant band-gap opening in graphene and Pd-doped graphene via the adsorption of ionized methane, Superlattices Microstruct. 104 (2017) 341–348, http://dx.doi.org/10.1016/j.spmi.2017.02.030.

[11] M.F. Craciun, I. Khrapach, M.D. Barnes, S. Russo, Properties and applications of chemically functionalized graphene, J. Phys.: Condens. Matter. 25 (42) (2013) 423201, http://dx.doi.org/10.1088/0953-8984/25/42/423201.

[12] M.G. Betti, E. Placidi, C. Izzo, E. Blundo, A. Polimeni, M. Sbroscia, J. Avila, P. Dudin, K. Hu, Y. Ito, D. Prezzi, M. Bonacci, E. Molinari, C. Mariani, Gap opening in double-sided highly hydrogenated free-standing graphene, Nano Lett. 22 (7) (2022) 2971–2977, http://dx.doi.org/10.1021/acs.nanolett.2c00162.

[13] S.Y. Zhou, G.-H. Gweon, A.V. Fedorov, P.N. First, W.A. de Heer, D.-H. Lee, F. Guinea, A.H. Castro Neto, A. Lanzara, Substrate-induced bandgap opening in epitaxial graphene, Nat. Mater. 6 (10) (2007) 770–775, http://dx.doi.org/10.1038/nmat2003.

[14] S. Tang, W. Wu, X. Xie, X. Li, J. Gu, Band gap opening of bilayer graphene by graphene oxide support doping, RSC Adv. 7 (2017) 9862–9871, http://dx.doi.org/10.1039/C7RA01134B.

[15] H. Kim, N. Leconte, B.L. Chittari, K. Watanabe, T. Taniguchi, A.H. MacDonald, J. Jung, S. Jung, Accurate gap determination in monolayer and bilayer graphene/h-BN Moiré superlattices, Nano Lett. 18 (12) (2018) 7732–7741, http://dx.doi.org/10.1021/acs.nanolett.8b03423.

[16] G. Giovannetti, P.A. Khomyakov, G. Brocks, P.J. Kelly, J. van den Brink, Substrate-induced band gap in graphene on hexagonal boron nitride: Ab initio density functional calculations, Phys. Rev. B 76 (2007) 073103, http://dx.doi.org/10.1103/PhysRevB.76.073103.

[17] M. N. Nair, I. Palacio, A. Celis, A. Zobelli, A. Gloter, S. Kubsky, J.-P. Turmaud, M. Conrad, C. Berger, W. de Heer, E.H. Conrad, A. Taleb-Ibrahimi, A. Tejeda, Band gap opening induced by the structural periodicity in epitaxial graphene buffer layer, Nano Lett. 17 (4) (2017) 2681–2689, http://dx.doi.org/10.1021/acs.nanolett.7b00509.

[18] T.-o. Terasawa, K. Matsunaga, N. Hayashi, T. Ito, S.-i. Tanaka, S. Yasuda, H. Asaoka, Band gap opening in graphene by hybridization with Au (001) reconstructed surfaces, Phys. Rev. Mater. 7 (2023) 014002, http://dx.doi.org/10.1103/PhysRevMaterials.7.014002.

[19] K.F. Mak, C.H. Lui, J. Shan, T.F. Heinz, Observation of an electric-field-induced band gap in bilayer graphene by infrared spectroscopy, Phys. Rev. Lett. 102 (2009) 256405, http://dx.doi.org/10.1103/PhysRevLett.102.256405.

[20] K. Kanayama, K. Nagashio, Gap state analysis in electric-field-induced band gap for bilayer graphene, Sci. Rep. 5 (1) (2015) 15789, http://dx.doi.org/10.1038/srep15789.

[21] S. Talkington, E.J. Mele, Electric-field-tunable band gap in commensurate twisted bilayer graphene, Phys. Rev. B 107 (2023) L041408, http://dx.doi.org/10.1103/PhysRevB.107.L041408.

[22] A. Boschi, Z.M. Gebeyehu, S. Slizovskiy, V. Mišeikis, S. Forti, A. Rossi, K. Watanabe, T. Taniguchi, F. Beltram, V.I. Fal'ko, C. Coletti, S. Pezzini, Built-in Bernal gap in large-angle-twisted monolayer-bilayer graphene, Commun. Phys. 7 (1) (2024) 391, http://dx.doi.org/10.1038/s42005-024-01887-0.

[23] R. Martinazzo, S. Casolo, G.F. Tantardini, Symmetry-induced band-gap opening in graphene superlattices, Phys. Rev. B 81 (2010) 245420, http://dx.doi.org/10.1103/PhysRevB.81.245420.

[24] J.C.W. Song, A.V. Shytov, L.S. Levitov, Electron interactions and gap opening in graphene superlattices, Phys. Rev. Lett. 111 (2013) 266801, http://dx.doi.org/10.1103/PhysRevLett.111.266801.

[25] S.L. Xiu, L. Gong, V. Wang, Y.Y. Liang, G. Chen, Y. Kawazoe, Degenerate perturbation in band-gap opening of graphene superlattice, J. Phys. Chem. C 118 (15) (2014) 8174–8180, http://dx.doi.org/10.1021/jp5002572.

[26] R. Balog, B. Jørgensen, L. Nilsson, M. Andersen, E. Rienks, M. Bianchi, M. Fanetti, E. Lægsgaard, A. Baraldi, S. Lizzit, Z. Sljivancanin, F. Besenbacher, B. Hammer, T.G. Pedersen, P. Hofmann, L. Hornekær, Bandgap opening in graphene induced by patterned hydrogen adsorption, Nat. Mater. 9 (4) (2010) 315–319, http://dx.doi.org/10.1038/nmat2710.

[27] A. Qadoos, M. Rashid, M. Naeem, Z. Jiang, M. Moin, M. Babar, Bandgap engineering in graphene oxide (GO) via integrating DFT calculations with atmospheric-pressure microplasma (AMP) treatment for optoelectronic applications, Hybrid Adv. 8 (2025) 100353, http://dx.doi.org/10.1016/j.hybadv.2024.100353.

[28] A. Hunt, E. Kurmaev, A. Moewes, Band gap engineering of graphene oxide by chemical modification, Carbon 75 (2014) 366–371, http://dx.doi.org/10.1016/j.carbon.2014.04.015.

[29] J.O. Sofo, A.S. Chaudhari, G.D. Barber, Graphane: A two-dimensional hydrocarbon, Phys. Rev. B 75 (2007) 153401, http://dx.doi.org/10.1103/PhysRevB.75.153401.

[30] M. Pumera, C.H.A. Wong, Graphane and hydrogenated graphene, Chem. Soc. Rev. 42 (2013) 5987–5995, http://dx.doi.org/10.1039/C3CS60132C.

[31] Y. Duan, C.D. Stinespring, B. Chorpening, Electronic structures, bonding configurations, and band-gap-opening properties of graphene binding with low-concentration fluorine, ChemistryOpen 4 (5) (2015) 642–650, http://dx.doi.org/10.1002/open.201500074.

[32] F. Li, Y. Li, Band gap modulation of janus graphene nanosheets by interlayer hydrogen bonding and the external electric field: a computational study, J. Mater. Chem. C 3 (2015) 3416–3421, http://dx.doi.org/10.1039/C5TC00013K.

[33] O. Leenaerts, H. Peelaers, A.D. Hernández-Nieves, B. Partoens, F.M. Peeters, First-principles investigation of graphene fluoride and graphane, Phys. Rev. B 82 (2010) 195436, http://dx.doi.org/10.1103/PhysRevB.82.195436.

[34] J. Jung, A.M. DaSilva, A.H. MacDonald, S. Adam, Origin of band gaps in graphene on hexagonal boron nitride, Nat. Commun. 6 (1) (2015) 6308, http://dx.doi.org/10.1038/ncomms7308.

[35] Y. Son, M.L. Cohen, S.G. Louie, Half-metallic graphene nanoribbons, Nature 444 (2006) 347, http://dx.doi.org/10.1038/nature05180.

[36] Y. Son, M.L. Cohen, S.G. Louie, Energy gaps in graphene nanoribbons, Phys. Rev. Lett. 97 (2006) 216803, http://dx.doi.org/10.1103/PhysRevLett.97.216803.

[37] N.V. Tepliakov, J. Lischner, E. Kaxiras, A.A. Mostofi, M. Pizzochero, Unveiling and manipulating hidden symmetries in graphene nanoribbons, Phys. Rev. Lett. 130 (2023) 026401, http://dx.doi.org/10.1103/PhysRevLett.130.026401.

[38] Y.Y. Li, M.X. Chen, M. Weinert, L. Li, Direct experimental determination of onset of electron–electron interactions in gap opening of zigzag graphene nanoribbons, Nat. Commun. 5 (1) (2014) 4311, http://dx.doi.org/10.1038/ncomms5311.

[39] H. Karakachian, T.T.N. Nguyen, J. Aprojanz, A.A. Zakharov, R. Yakimova, P. Rosenzweig, C.M. Polley, T. Balasubramanian, C. Tegenkamp, S.R. Power, U. Starke, One-dimensional confinement and width-dependent bandgap formation in epitaxial graphene nanoribbons, Nat. Commun. 11 (1) (2020) 6380, http://dx.doi.org/10.1038/s41467-020-19051-x.

[40] N. Merino-Díez, A. Garcia-Lekue, E. Carbonell-Sanromà, J. Li, M. Corso, L. Colazzo, F. Sedona, D. Sánchez-Portal, J.I. Pascual, D.G. de Oteyza, Width-dependent band gap in armchair graphene nanoribbons reveals Fermi level pinning on Au(111), ACS Nano 11 (11) (2017) 11661–11668, http://dx.doi.org/10.1021/acsnano.7b06765.

[41] A. Tries, S. Osella, P. Zhang, F. Xu, C. Ramanan, M. Kläui, Y. Mai, D. Beljonne, H.I. Wang, Experimental observation of strong exciton effects in graphene nanoribbons, Nano Lett. 20 (5) (2020) 2993–3002, http://dx.doi.org/10.1021/acs.nanolett.9b04816.

[42] Y.-M. Lin, V. Perebeinos, Z. Chen, P. Avouris, Electrical observation of subband formation in graphene nanoribbons, Phys. Rev. B 78 (2008) 161409, http://dx.doi.org/10.1103/PhysRevB.78.161409.

[43] G. Borin Barin, A. Fairbrother, L. Rotach, M. Bayle, M. Paillet, L. Liang, V. Meunier, R. Hauert, T. Dumslaff, A. Narita, K. Müllen, H. Sahabudeen, R. Berger, X. Feng, R. Fasel, P. Ruffieux, Surface-synthesized graphene nanoribbons for room temperature switching devices: Substrate transfer and ex situ characterization, ACS Appl. Nano Mater. 2 (4) (2019) 2184–2192, http://dx.doi.org/10.1021/acsanm.9b00151.

[44] K.K. Gopalan, B. Paulillo, D.M. Mackenzie, D. Rodrigo, N. Bareza, P.R. Whelan, A. Shivayogimath, V. Pruneri, Scalable and tunable periodic graphene nanohole arrays for mid-infrared plasmonics, Nano Lett. 18 (9) (2018) 5913–5918, http://dx.doi.org/10.1021/acs.nanolett.8b02613.

[45] H. Kuzmany, L. Shi, M. Martinati, S. Cambré, W. Wenseleers, J. Kürti, J. Koltai, G. Kukucska, K. Cao, U. Kaiser, T. Saito, T. Pichler, Well-defined sub-nanometer graphene ribbons synthesized inside carbon nanotubes, Carbon 171 (2021) 221–229, http://dx.doi.org/10.1016/j.carbon.2020.08.065.

[46] T.G. Pedersen, C. Flindt, J. Pedersen, N.A. Mortensen, A.-P. Jauho, K. Pedersen, Graphene antidot lattices: Designed defects and spin qubits, Phys. Rev. Lett. 100 (2008) 136804, http://dx.doi.org/10.1103/PhysRevLett.100.136804.

[47] J.A. Fürst, J.G. Pedersen, C. Flindt, N.A. Mortensen, M. Brandbyge, T.G. Pedersen, A.-P. Jauho, Electronic properties of graphene antidot lattices, New J. Phys. 11 (9) (2009) 095020, http://dx.doi.org/10.1088/1367-2630/11/9/095020.

[48] F. Ouyang, S. Peng, Z. Liu, Z. Liu, Bandgap opening in graphene antidot lattices: The missing half, ACS Nano 5 (5) (2011) 4023–4030, http://dx.doi.org/10.1021/nn200580w.

[49] Y. Pan, H. Lv, X. Wu, Topologically frustrated graphene antidot lattice semiconductors with room-temperature magnetism, J. Phys. Chem. C 127 (6) (2023) 3276–3284, http://dx.doi.org/10.1021/acs.jpcc.2c08075.

[50] M. Vanević, V.M. Stojanović, M. Kindermann, Character of electronic states in graphene antidot lattices: Flat bands and spatial localization, Phys. Rev. B 80 (2009) 045410, http://dx.doi.org/10.1103/PhysRevB.80.045410.

[51] Y. Taguchi, M. Toyoda, S. Saito, Electronic properties of graphene with triangular defects in a superhoneycomb arrangement: A first-principles study, Phys. Rev. B 107 (2023) 235418, http://dx.doi.org/10.1103/PhysRevB.107.235418.

[52] S. Xiu, M. Zheng, P. Zhao, Y. Zhang, H. Liu, S. Li, G. Chen, Y. Kawazoe, An effective method of tuning conducting properties: First-principles studies on electronic structures of graphene nanomeshes, Carbon 79 (1) (2014) 646–653, http://dx.doi.org/10.1016/j.carbon.2014.08.050.

[53] S. Yuan, R. Roldán, A.-P. Jauho, M.I. Katsnelson, Electronic properties of disordered graphene antidot lattices, Phys. Rev. B 87 (2013) 085430, http://dx.doi.org/10.1103/PhysRevB.87.085430.

[54] S.R. Power, A.-P. Jauho, Electronic transport in disordered graphene antidot lattice devices, Phys. Rev. B 90 (11) (2014) 115408, http://dx.doi.org/10.1103/PhysRevB.90.115408.

[55] T. Wei, F. Hauke, A. Hirsch, Evolution of graphene patterning: From dimension regulation to molecular engineering, Adv. Mater. 33 (45) (2021) 2104060, http://dx.doi.org/10.1002/adma.202104060.

[56] Q. Sun, M. Dai, J. Hong, S. Feng, C. Wang, Z. Yuan, Graphene nanopore fabrication and applications, Int. J. Mol. Sci. 26 (4) (2025) http://dx.doi.org/10.3390/ijms26041709.

[57] S. Standop, O. Lehtinen, C. Herbig, G. Lewes-Malandrakis, F. Craes, J. Kotakoski, T. Michely, A.V. Krasheninnikov, C. Busse, Ion impacts on graphene/Ir(111): Interface channeling, vacancy funnels, and a nanomesh, Nano Lett. 13 (5) (2013) 1948–1955, http://dx.doi.org/10.1021/nl304659n.

[58] G.F. Schneider, S.W. Kowalczyk, V.E. Calado, G. Pandraud, H.W. Zandbergen, L.M.K. Vandersypen, C. Dekker, DNA translocation through graphene nanopores, Nano Lett. 10 (8) (2010) 3163–3167, http://dx.doi.org/10.1021/nl102069z.

[59] M.D. Fischbein, M. Drndić, Electron beam nanosculpting of suspended graphene sheets, Appl. Phys. Lett. 93 (11) (2008) 113107, http://dx.doi.org/10.1063/1.2980518.

[60] K. He, A.W. Robertson, C. Gong, C.S. Allen, Q. Xu, H. Zandbergen, J.C. Grossman, A.I. Kirkland, J.H. Warner, Controlled formation of closed-edge nanopores in graphene, Nanoscale 7 (2015) 11602–11610, http://dx.doi.org/10.1039/C5NR02277K.

[61] X. Zhao, J. Kotakoski, J.C. Meyer, E. Sutter, P. Sutter, A.V. Krasheninnikov, U. Kaiser, W. Zhou, Engineering and modifying two-dimensional materials by electron beams, MRS Bull. 42 (2017) 667–676, http://dx.doi.org/10.1557/mrs.2017.184.

[62] O. Cretu, H.-p. Komsa, O. Lehtinen, G. Algara-Siller, U. Kaiser, K. Suenaga, A.V. Krasheninnikov, Experimental observation of boron nitride chains, ACS Nano 8 (2014) 11950–11957.

[63] A.V. Krasheninnikov, F. Banhart, Engineering of nanostructured carbon materials with electron or ion beams, Nat. Mater. 6 (2007) 723–733, http://dx.doi.org/10.1038/nmat1996.

[64] A.W. Robertson, G.-D. Lee, K. He, Y. Fan, C.S. Allen, S. Lee, H. Kim, E. Yoon, H. Zheng, A.I. Kirkland, J.H. Warner, Partial dislocations in graphene and their atomic level migration dynamics, Nano Lett. 15 (9) (2015) 5950–5955, http://dx.doi.org/10.1021/acs.nanolett.5b02080.

[65] C.S. Boland, Y. Sun, D.G. Papageorgiou, Bandgap engineering of 2D materials toward high-performing straintronics, Nano Lett. 24 (41) (2024) 12722–12732, http://dx.doi.org/10.1021/acs.nanolett.4c03321.

[66] J. Martín-Sánchez, R. Trotta, A. Mariscal, R. Serna, G. Piredda, S. Stroj, J. Edlinger, C. Schimpf, J. Aberl, T. Lettner, J. Wildmann, H. Huang, X. Yuan, D. Ziss, J. Stangl, A. Rastelli, Strain-tuning of the optical properties of semiconductor nanomaterials by integration onto piezoelectric actuators, Semicond. Sci. Technol. 33 (1) (2017) 013001, http://dx.doi.org/10.1088/1361-6641/aa9b53.

[67] G.H. Ahn, et al., Strain-engineered growth of two-dimensional materials, Nat. Commun. 8 (2017) 608, http://dx.doi.org/10.1038/s41467-017-00516-5.

[68] S. Bertolazzi, J. Brivio, A. Kis, Stretching and breaking of ultrathin MoS 2, ACS Nano 5 (2011) 9703–9709, http://dx.doi.org/10.1021/nn203879f.

[69] C. Palacios-Berraquero, D.M. Kara, A.R. Montblanch, M. Barbone, P. Latawiec, D. Yoon, A.K. Ott, M. Loncar, A.C. Ferrari, M. Atatüre, Large-scale quantum-emitter arrays in atomically thin semiconductors, Nat. Commun. 8 (1) (2017) 15093, http://dx.doi.org/10.1038/ncomms15093.

[70] C. Herbig, E.H. Åhlgren, U.A. Schröder, A.J. Martínez-Galera, M.A. Arman, J. Kotakoski, J. Knudsen, A.V. Krasheninnikov, T. Michely, Xe irradiation of graphene on Ir(111): From trapping to blistering, Phys. Rev. B 92 (8) (2015) 085429, http://dx.doi.org/10.1103/PhysRevB.92.085429.

[71] H.J. Conley, B. Wang, J.I. Ziegler, R.F. Haglund, S.T. Pantelides, K.I. Bolotin, Bandgap engineering of strained monolayer and bilayer MoS2, Nano Lett. 13 (8) (2013) 3626–3630, http://dx.doi.org/10.1021/nl4014748.

[72] A.V. Tyurnina, D.A. Bandurin, E. Khestanova, V.G. Kravets, M. Koperski, F. Guinea, A.N. Grigorenko, A.K. Geim, I.V. Grigorieva, Strained bubbles in van der waals heterostructures as local emitters of photoluminescence with adjustable wavelength, ACS Photonics 6 (2) (2019) 516–524, http://dx.doi.org/10.1021/acsphotonics.8b01497.

[73] A.A. Shokri, E.K. Safari, Ab-initio study of planar strain on electronic structure properties of graphene sheets with nanoholes, Indian J. Phys. 89 (2015) 23–29, http://dx.doi.org/10.1007/s12648-014-0534-2.

[74] B. Song, G.G.F.G. Schneider, Q. Xu, G. Pandraud, C. Dekker, H. Zandbergen, Atomic-scale electron-beam sculpting of near-defect-free graphene nanostructures, Nano Lett. 11 (6) (2011) 2247–2250, http://dx.doi.org/10.1021/nl200369r.

[75] J.P. Perdew, K. Burke, M. Ernzerhof, Generalized gradient approximation made simple, Phys. Rev. Lett. 77 (18) (1996) 3865–3868, http://dx.doi.org/10.1103/physrevlett.77.3865.

[76] G. Kresse, D. Joubert, From ultrasoft pseudopotentials to the projector augmented-wave method, Phys. Rev. B 59 (3) (1999) 1758–1775, http://dx.doi.org/10.1103/physrevb.59.1758.

[77] G. Kresse, J. Furthmüller, Efficient iterative schemes for *ab initio* total-energy calculations using a plane-wave basis set, Phys. Rev. B 54 (16) (1996) 11169–11186, http://dx.doi.org/10.1103/physrevb.54.11169.

[78] J.J. Jorgensen, G.L.W. Hart, Effectiveness of smearing and tetrahedron methods: best practices in DFT codes, Modelling Simul. Mater. Sci. Eng. 29 (6) (2021) 065014, http://dx.doi.org/10.1088/1361-651X/ac13ca.

[79] J. Hafner, Ab-initio simulations of materials using VASP: Density-functional theory and beyond, J. Comput. Chem. 29 (13) (2008) 2044–2078, http://dx.doi.org/10.1002/jcc.21057.

[80] M.Y. Toriyama, A.M. Ganose, M. Dylla, S. Anand, J. Park, M.K. Brod, J. Munro, K.A. Persson, A. Jain, G.J. Snyder, Comparison of the tetrahedron method to smearing methods for the electronic density of states, 2021.

[81] K. Momma, F. Izumi, *VESTA3* for three-dimensional visualization of crystal, volumetric and morphology data, J. Appl. Crystallogr. 44 (6) (2011) 1272–1276, http://dx.doi.org/10.1107/S0021889811038970.

[82] V. Wang, N. Xu, J.-C. Liu, G. Tang, W.-T. Geng, VASPKIT: A user-friendly interface facilitating high-throughput computing and analysis using VASP code, Comput. Phys. Comm. 267 (2021) 108033, http://dx.doi.org/10.1016/j.cpc.2021.108033.

[83] F. Ouyang, Z. Yang, S. Peng, X. Zheng, X. Xiong, Antidot-dependent bandgap and clar sextets in graphene antidot lattices, Phys. E 56 (2014) 222–226, http://dx.doi.org/10.1016/j.physe.2013.09.006.

[84] F. Ouyang, S. Peng, Z. Yang, Y. Chen, H. Zou, X. Xiong, Bandgap opening/closing of graphene antidot lattices with zigzag-edged hexagonal holes, Phys. Chem. Chem. Phys. 16 (2014) 20524–20531, http://dx.doi.org/10.1039/C4CP02090A.

[85] H. Jippo, M. Ohfuchi, C. Kaneta, Theoretical study on electron transport properties of graphene sheets with two- and one-dimensional periodic nanoholes, Phys. Rev. B 075467 (2011) 075467, http://dx.doi.org/10.1103/PhysRevB.84.075467.

[86] P. Koskinen, S. Malola, H. Hakkinen, Self-passivating edge reconstructions of graphene, Phys. Rev. Lett. 101 (11) (2008) 115502, http://dx.doi.org/10.1103/PhysRevLett.101.115502.

[87] J.P. Perdew, Density functional theory and the band gap problem, Int. J. Quantum Chem. 28 (S19) (1985) 497–523, http://dx.doi.org/10.1002/qua.560280846.

[88] J. Pető, G. Dobrik, G. Kukucska, P. Vancsó, A.A. Koós, J. Koltai, P. Nemes-Incze, C. Hwang, L. Tapasztó, Moderate strain induced indirect bandgap and conduction electrons in MoS2 single layers, Npj 2D Mater. Appl. 3 (1) (2019) 39, http://dx.doi.org/10.1038/s41699-019-0123-5.

[89] B. Mondal, R. Tonner-Zech, Systematic strain-induced bandgap tuning in binary III–V semiconductors from density functional theory, Phys. Scr. 98 (6) (2023) 065924, http://dx.doi.org/10.1088/1402-4896/acd08b.

[90] J.A. Fürst, T.G. Pedersen, M. Brandbyge, A.-P. Jauho, Density functional study of graphene antidot lattices: Roles of geometrical relaxation and spin, Phys. Rev. B 80 (2009) 115117, http://dx.doi.org/10.1103/PhysRevB.80.115117.

[91] G. Gui, J. Li, J. Zhong, Band structure engineering of graphene by strain: First-principles calculations, Phys. Rev. B 78 (2008) 075435, http://dx.doi.org/10.1103/PhysRevB.78.075435.

[92] X.Y. Cui, R.K. Zheng, Z.W. Liu, L. Li, B. Delley, C. Stampfl, S.P. Ringer, Magic numbers of nanoholes in graphene: Tunable magnetism and semiconductivity, Phys. Rev. B 84 (2011) 125410, http://dx.doi.org/10.1103/PhysRevB.84.125410.

[93] O. Yazyev, Emergence of magnetism in graphene materials and nanostructures, Rep. Progr. Phys. 73 (5) (2010) 056501, http://dx.doi.org/10.1088/0034-4885/73/5/056501.

[94] F. Banhart, J. Kotakoski, A.V. Krasheninnikov, Structural defects in graphene, ACS Nano 5 (1) (2011) 26–41, http://dx.doi.org/10.1021/nn102598m.

[95] S. Wang, B. Yang, J. Yuan, Y. Si, H. Chen, Large-scale molecular simulations on the mechanical response and failure behavior of a defective graphene: Cases of 5–8–5 defects, Sci. Rep. 5 (1) (2015) 14957, http://dx.doi.org/10.1038/srep14957.

[96] P.Y. Huang, C.S. Ruiz-Vargas, A.M. van der Zande, W.S. Whitney, M.P. Levendorf, J.W. Kevek, S. Garg, J.S. Alden, C.J. Hustedt, Y. Zhu, J. Park, P.L. McEuen, D.A. Muller, Grains and grain boundaries in single-layer graphene atomic patchwork quilts, Nature 469 (7330) (2011) 389–392, http://dx.doi.org/10.1038/nature09718.

[97] X. Qin, Q. Meng, Y. Feng, Y. Gao, Graphene with line defect as a membrane for gas separation: Design via a first-principles modeling, Surf. Sci. 607 (2013) 153–158, http://dx.doi.org/10.1016/j.susc.2012.08.024.

[98] D. Berger, C. Ratsch, Line defects in graphene: How doping affects the electronic and mechanical properties, Phys. Rev. B 93 (2016) 235441, http://dx.doi.org/10.1103/PhysRevB.93.235441.